RSC Advances

ROYAL SOCIETY OF CHEMISTRY

www.rsc.org/advances

Efficient removal of U(VI) from aqueous solutions by polyaniline/hydrogen-titanate nanobelt composites

Yan Liu[1], Yuying Yang[1], Lei Chen[1]*, Hongshan Zhu[1], Yunhui Dong[1]*, Njud S. Alharbi[2], Ahmed Alsaedi[3], Jun Hu[1,3]

1. School of Chemical Engineering, Shandong University of Technology, 255049, Zibo, Shandong, P. R. China
2. Biotechnology Research Group, Department of Biological Sciences, Faculty of Science, King Abdulaziz University, Jeddah, Saudi Arabia
3. NAAM Research Group, Department of Mathematics, Faculty of Science, King Abdulaziz University, Jeddah, Saudi Arabia

*: Corresponding author: Email address: chenleily7612@163.com (L. Chen), Fax: +86-533-2781664; Tel: +86-533-2781664

Abstract

The organic-inorganic hybrid material of polyaniline/hydrogen-titanate nanobelt (PANI/H-TNB) composites were fabricated through a convenience oxidative polymerization approach. The characteristic results of X-ray powder diffraction and Fourier transformed infrared spectroscopy showed that aniline was successfully polymerized onto titanate surfaces. The adsorption capacity of PANI/H-TNB composites toward U(VI) was evaluated by batch experiments, and this adsorption process followed pseudo-second order kinetics model and Langmuir model. The PANI/H-TNB composites showed an maximum adsorption amount of 216.82 mg/g toward U(VI), which was higher that PANI (48.75 mg/g) and many other adsorbents. The thermodynamic parameters calculated from adsorption isotherms indicated a spontaneous and endothermic adsorption process. Higher adsorption capacities were observed after regeneration for six cycles. The PANI/H-TNB composites could be regarded as a potential adsorbent to remove U(VI) from wastewater.

Keywords: Polyaniline; Adsorption; U(VI); Titanate

1. Introduction

The nuclear industry, especially nuclear power program in chian, is developing rapidly recently. Large quantities of hazardous radionuclides have been generated and possibly discharged into the nature water [1], which result in serious environmental pollution. Uranium, one of the most predominant radionuclide contaminants, and produced nuclear fuel production, ore mining, weapons manufacturing and research activities, is quite stable in soils and groundwater [2, 3]. Under normal environmental conditions, uranium exists mainly as the uranyl cation UO_2^{2+} in aqueous solutions, which offers the possibility for the removal of the U(VI) ions onto solid materials for effective separation and enrichment [4]. Uranium contaminations, which are discharged into the environment, could cause a threat to human health and ecological systems due to their toxicity and radioactivity [5, 6]. Thus it is necessary to develop advanced technologies to remove uranium from the aqueous solutions before they are discharged into the environment.

Currently, various technologies have been proposed to remove U(VI) from wastewater, such as precipitation, membrane filtration, adsorption, ion exchange and etc [7-10]. The adsorption technique is regarded as one of feasible and environment-friendly methods because of the low cost, simple design and operation [11, 12]. However, the limited adsorption capacity restricts their practical application for the removal of U(VI) from aqueous solutions. Therefore, it is an urgent to design new adsorbents with excellent stabilities and high adsorption capacities to remove U(VI) from aqueous wastes [13].

In recent years, the nanocomposites based on organic-inorganic hybrid for adsorbent have been attracting widespread concern due to their potential adsorption capacity and unique functionality. For example, Gao et al. [14] reported that a novel organic-inorganic hybrid of polyaniline/titanium phosphate holds a good adsorption capacity toward Re(VII). Pérez et al. [15] found that the synthesis of organic-inorganic interpenetrated hybrids based on cationic polymer and hydrous zirconium oxide composites exhibited excellent adsorption capacity for arsenic from wastewater. Wang et al. [16] found that organic-inorganic hybrid of polyaniline/α-zirconium phosphate performed a good adsorption behavior for the removal of organic pollutants from aqueous solutions. However, the investigative of the organic-inorganic hybrid materials for adsorption is still required for practical utility. Polyaniline (PANI) is an easy produced and low cost polymer with excellent chemical stability and adjustable electrical conductivity [17-20]. With its primary and secondary amino functional groups, PANI is expected to exhibite a strong affinity with heavy metal ions in water [14, 21]. Titanates have a unique micro structure that can produce a high adsorption capacity via ionic exchanges [22]. We combined the organic PANI with the inorganic hydrogen titanate nanobelt to obtain PANI/ hydrogen titanate nanobelt (PANI/H-TNB) composites, which may retain the best properties of PANI and adsorption capacity of titanate [23]. Therefore, it would be of great interest to synthesize this organic-inorganic hybrid material of PANI/H-TNB composites for wastewater treatment.

In this work, organic-inorganic hybrid materials of PANI/H-TNB composites were synthesized by in site polymerizing aniline onto the surface of titanate. The

PANI/H-TNB composites were characterized by scanning electron microscopy (SEM), transmission electron microscopy (TEM), Fourier transform infrared(FT-IR) spectroscopy, powder X-ray diffraction (XRD), and Zeta potential. Batch experiments were adopted to assess the removal performance of PANI/H-TNB composites toward U(VI) under various conditions. The influencing factors such as contact time, ionic strength ,solid content, pH value, were investigated. Besides, the repeated practicability was also carried out to estimate the possible practical applications.

2. Materials and method

2.1. Materials

Titania P_{25} (TiO_2; ca. 80% anatase and 20% rutile) was used as the titanium source. All other chemicals were purchased from Sinopharm Chemical Reagent Co. Ltd at analytically pure grade and used directly without further treatment.

2.2 Synthesis PANI/H-TNB composites

Titanate nanobelts were prepared according to previous study [24]. P_{25} powder (1.0 g) was added into 5 mol/L NaOH (80 mL) aqueous solution, which was then placed in 100 mL an airtight steel container. The mixture was heated to and maintained at 200 °C for 96 h. After cooling to room temperature, the solid was obtained by filtration and further washed with deionized water, and washed with dilute HCl to neutralize it. After that, the product dried in vacuum at 60 °C for 8 h to obtained the desired H-TNB.

The PANI/H-TNB composites were prepared via self-assembly method, as detailed in previous study [25]. Firstly, H-TNB(80 mg), aniline (6 mmol) and phytic acid

(PA, 1.8 mmol) were added into in 50 mL deionized water with magnetic stirring for 1 h at room temperature. Then, 30 mL of 0.2 mol/L ammonium peroxydisulfate ($(NH_4)_2S_2O_8$, APS) precooled with an ice bath for 5 min was added into the above mixture. The reaction was performed in the ice-water bath and stirred vigorously for about 20 h. The PANI/H-TNB composites were obtained by filtration and further washed with deionized water and ethanol for several times finally dried at 60 °C under vacuum for 24 h.

2.3 Material characterization

The PANI/H-TNB composites were characterized by SEM, TEM, XRD, FT-IR, and zeta potentials. The SEM images were obtained by using a JEOL JSM-6330F instrument operated at the beam energy of 15.0 kV and the TEM images were recorded with a JEOL-2010 microscope. The XRD patterns were obtained with CuKα radiation (λ = 1.5406 Å) of 10-70° with a step size of 0.02° and a count time of 8 s. The FTIR spectra were recorded in pressed KBr pellets (Aldrich, 99%, analytical reagent) over a range from 400 to 4000 cm^{-1}. The zeta potentials of PANI/H-TNB composites were measured on a Malvern ZEN2600 Zetasizer.

2.4 Adsorption experiments

Adsorption experiments were carried out in polyethylene centrifuge tubes with 0.3 g/L PANI/H-TNB composites and 20 mg/L U(VI) solutions. The background electrolyte solution of 0.1 mol/L $NaNO_3$ was prepared to achieve the desired ionic strength. Negligible volume of 0.1-1.0 mol/L HNO_3 or NaOH solution was added into the suspension solutions to adjust pH to the desired values. To achieve the adsorption

equilibrium, the tubes were placed on an oscillator and kept shaking for 24 h, then the solutions were centrifuged at 8000 rpm for 15 min. The concentration of U(VI) was measured by the Dichlorophosphonoazo III Spectrophotometer (V-1600 Mapada Shanghai) at the wavelength of 669 nm. The amount of U(VI) adsorbed on PANI/H-TNB can be calculated from the difference between the initial (C_0) and the equilibrium concentration (C_e) of the U(VI) solutions. The adsorption was expressed in terms of adsorption percentage (%) and distribution coefficient (K_d), which were calculated from the following equations:

$$Adsorption = \frac{C_0 - C_e}{C_0} \times 100\% \quad (1)$$

$$K_d = \frac{C_0 - C_e}{C_e} \times \frac{V}{m} \quad (2)$$

where C_0 (mg/L) is the initial concentration, C_e (mg/L) is the equilibrium concentration of U(VI) after adsorption. m (g) is the mass of PANI/H-TNB, and V (L) represents the volume of the suspension. The relative errors of data were less than ± 5%.

3. Results and discussion

3.1. Characterization

The surface morphologies of PANI and PANI/H-TNB composites were characterized by SEM (Fig. 1a and 1b) and TEM technique (Fig. 1c and 1d). Fig. 1a displayed that PANI performed as piles of nanofibers was aggregated loosely and arranged in a disordered structure. These disordered structured composites were considered to have a potential capacity for water treatment including the removal of

heavy metal ions [26]. Compared to PANI nanotubes, the PANI/H-TNB composites became wrinkled and crumpled structure, and much more rough, indicating PANI covered on the surfaces of nanobelts (Fig. 1b). Fig. 1c showed that PANI nanostructures are composed of nanowires and nanotubes that are roughly surfaced, which means the surface area of such kind of PANI nanowires/tubes is larger. Fig. 1d demonstrated that the PANI/H-TNB composites had an obvious core-shell structure.

The as-prepared of H-TNB, PANI, and PANI/H-TNB composites were characterized by XRD (Fig. 2). The main peaks at 2θ = 11.78, 24.93, 28.24, 33.63, 36.12, 43.45 and 48.36° corresponded to the (200), (110), (310), (112), (312), (204) and (020) planes of the H-TNB, respectively. The XRD pattern of H-TNB was in good agreement with the standard diffraction data (JCPDS no. 44-0131) [27]. Two new broad peaks of PANI/H-TNB composites were observed at 2θ = 20.46 and 25.82°, which was almost the same as those of pure PANI nanorods [28]. The results suggested that the PANI was successfully grafted on hydrogen titanate.

Fig. 3 showed the FTIR spectrum of H-TNB, PANI and PANI/H-TNB. In the FTIR spectrum of PANI, the characteristic bands at 1572, 1495, 1300 and 1127 cm^{-1} were attributed to the stretching vibrations of C–N bonds in N=Q=N, N–B–N, B–NH–B, and B–NH^{+}=Q (Q, quinoid ring; B, benzenoid ring), respectively [29]. The characteristic peaks at 658 and 480 cm^{-1} corresponded to Ti–O–Ti asymmetric and symmetric stretching modes, respectively, in the H-TNB spectrum. As for PANI/H-TNB composites, similar peaks at 1572, 1495 and 1300 cm^{-1} were observed from PANI, indicating the successful modifying of PANI on H-TNB to form

PANI/H-TNB.

As shown in Fig. 4a, the presence of U4f in PANI/H-TNB-U obviously demonstrated the adsorption of U(VI) on PANI/H-TNB surface after adsorption equilibrium [30]. For the PANI/H-TNB sample after the reaction (Fig. 4b), the XPS spectrum of $U4f_{5/2}$ and $U4f_{7/2}$ clearly displayed peaks at 393.2 and 382.4 eV, respectively [31, 32]. The adsorbed U was only detected in the oxidation state of U(VI) (Eb = 382.2 ± 0.3 and 393.1 ± 0.3 eV), and no reduced state of U(IV) (Eb = 380.4 ± 0.3 and 391.3 ± 0.3 eV) was detected, suggesting no chemical reduction was occurring.

Fig. 5 showed the zeta-potential values of PANI and PANI/H-TNB as a function of pH values. The zeta potentials of PANI was observed at about 8.3. The zeta potentials of PANI/H-TNB composites increased with decreasing pH values, which can be explained by the protonation of amino functional groups of PANI on PANI/H-TNB surfaces. The electrostatic point of PANI/H-TNB is measured at about 5.8, suggesting a positively charged surface at pH < 5.8 and a negatively charged surface at pH > 5.8.

3.2. Effect of contact time

Fig. 6. showed the adsorption kinetics of U(VI) on PANI/H-TNB composites. A relatively fast adsorption was observed within the first 5 h, and reached equilibrium after 5 h. To ensure adsorption equilibrium, a contact time of 24 h was selected for further experiments. This relatively fast adsorption equilibrium indicated that chemisorption and inner-sphere surface complexation were the main interaction

mechanisms of U(VI) with the composites [33].

In order to analyze interaction mechanisms in detail, the adsorption kinetics of U(VI) on PANI/H-TNB composites were fitted by pseudo-first order and pseudo-second-order kinetic models. The pseudo-first-order [34] and the pseudo-second-order [35] can be given in equations:

$$\ln(q_e - q_t) = \ln q_e - k_1 t \quad (3)$$

$$\frac{t}{q_t} = \frac{1}{k_2 q_t^2} + \frac{1}{q_e} t \quad (4)$$

where q_e and q_t (mg/g) are the amount of U(VI) adsorbed at equilibrium and at time t, respectively.

Parameters of adsorption kinetics were summarized in Table 1. A higher correlation coefficients (R^2) was observed for the pseudo-second-order model (0.999) than the pseudo-first-order model (0.885), indicating a pseudo-second-order adsorption process in this case. This result further corroborated the dominant chemisorption or strong surface complexation mechanism for the adsorption of U(VI) on PANI/H-TNB composites.

3.3. The effect of solid content amount

The effect of adsorbent content was shown in Fig. 7. Increased adsorption efficiencies were obtained with increasing amount of PANI/H-TNB composites. This phenomenon as was expected, and can be explained by the fact that the increasing content of PANI/H-TNB provided more available functional groups, which led to the available sites for the binding of U(VI). The distribution coefficient (K_d) was also provided in Fig. 7, which slowly decreased with the increase of PANI/H-TNB content.

With a low adsorbent content, the surface active sites were entirely exposed for adsorption and the surface was highly saturated, leading to a high distribution coefficient. However, the competition among the adsorption sites increased at high adsorbent concentrations, which could decrease the K_d values of U(VI). Similar adsorption behaviors of U(VI) were reported by Song et al. [36]and Zhao et al [37].

3.4. Effects of pH and ionic strength

The effect of pH values toward U(VI) adsorption was investigated and plotted in Fig. 8b. The adsorption efficiency increased with increasing pH values from 2.0 to 5.0, and kept the high level at pH 5.0-6.0, then decreased at higher pH value. This phenomenon was in accordance with the adsorption behavior of U(VI) on phosphate-functionalized graphene oxide [38], which was dependent on the species of U(VI) (Fig. 8a) and the surface properties of PANI/H-TNB composites at different pH values [39]. As illustrated in Fig. 8a, U(VI) mainly existed as UO_2^{2+} at pH < 5, and then predominant species such as $UO_2(OH)^+$, $(UO_2)_4(OH)_7^+$, $(UO_2)_3(OH)_5^+$ were formed at pH 5.0-7.0. Negatively charged species, such as $UO_2(OH)_3^-$, $UO_2(OH)_4^{2-}$ and $(UO_2)_3(OH)_7^-$ appeared and dominated at pH >7.0. As shown in Fig.5, the isoelectric point of PANI/H-TNB composites was calculated to be 5.8. Therefore, the electrostatic repulsion between positively charged PANI/H-TNB surfaces and UO_2^{2+} led to the low adsorption efficiencies at pH < 5. As the pH value increased, the surface of PANI/H-TNB composites was gradually negatively charged, resulting in the increased adsorption efficiencies. At pH = 5.0-6.0, the electrostatic attractions between the negatively charged PANI/H-TNB surfaces and positively charged U(VI)

species dominated, leading to the highest adsorption efficiencies. At pH > 7.0, negatively charged U(VI) appeared, promoting the electron repulsion with the negatively charged PANI/H-TNB surfaces, resulting in decreased adsorption efficiencies.

The effect of ionic strength was also measured at three different concentrations, i.e. 0.001, 0.01 and 0.1 M $NaNO_3$ solution, as shown in Fig. 8b, which indicated an independent ionic strength effect toward U(VI) adsorption within the measured pH values, suggesting a dominant inner-surface complexation mechanism rather than an outer-sphere surface complexation or ion exchange mechanism [8, 40].

3.5. Effect of coexisting ions

Various components simultaneously exist in aqueous solutions. To research the influence of coexisting ions on U(VI) adsorption, the adsorption of U(VI) on PANI/H-TNB composites was carried out in 0.01 mol/L solution, such as $NaClO_4$, $NaNO_3$, NaCl, Na_2SO_4, KNO_3, $Ca(NO_3)_2$and $Mg(NO_3)_2$, as a function of pH values. The effect of cationic ions was illustrated in Fig. 9a by comparing three cationic solutions, i.e., $NaNO_3$, KNO_3, $Ca(NO_3)_2$ and $Mg(NO_3)_2$. No obvious adsorption effects were observed. Positively charged cations may alter the surface property of PANI/H-TNB composites. However, one can see herein that the adsorption of U(VI) on PANI/H-TNB composites was not influenced obviously in the presence of three different cations, indicating that the uptake of U(VI) was mainly controlled by inner-sphere surface complexation.

Meanwhile, the anionic ions effects were shown in Fig. 9b by measuring in three

different solutions, i.e., NaCl, $NaNO_3$, Na_2SO_4 and $NaClO_4$. An obvious anionic ions effect was observed. The highest adsorption capacity was obtained in 0.01 M $NaClO_4$ solution, as compared with NaCl, $NaNO_3$ and Na_2SO_4 solutions, which was consistent with previous studies [8, 41]. This phenomenon indicated that the negatively charged anions with high chemical affinity and strong complexation ability towards both metal ions and solid surfaces, could obviously influence the mobility of metal ions in aqueous solutions. The Cl^-, NO_3^- and SO_4^{2-} ions could form soluble complexes with U(VI) (e.g., UO_2Cl^+, $UO_2NO_3^+$, $UO_2(SO_4)_2^{2-}$ species) whereas the ClO_4^- could not form stable complexes, hence leading to the decrease of U(VI) adsorption on PANI/H-TNB composites.

3.6. Effect of soil humic/fulvic acid

The influence of HA/FA on U(VI) adsorption to PANI/H-TNB composites as a function of pH was shown in Fig. 10. Slightly positive effects were observed for both HA and FA at pH < 6.0, while negative effects were found at pH > 6.0. At low pH values, the negatively charged HA/FA could be readily adsorbed on the positively charged surfaces of PANI/H-TNB composites. This adsorption will partially neutralize the positively charged PANI/H-TNB surfaces, promoting the adsorption of positively charged U(VI) species. Thus, positive effects were obtained. However, at high pH values, the PANI/H-TNB surfaces were getting negatively charged, which made it difficult to adsorb the negatively charged HA/FA. On the contrary, the free HA/FA molecules will interacted with U(VI) to form complexes of HA/FA-U(VI) in aqueous solution, resulting in an overall decrease in U(VI) adsorption. It was very

interesting to note that the influence of FA on U(VI) adsorption to PANI/H-TNB was similar to that of U(VI) in the presence of HA. Both FA and HA had a macromolecular structure [42, 43] and could be described as aggregates of aromatic molecules (mostly phenolic) carrying a large number of functional groups. The samples of HA and FA were obtained from the same material and they possessed similar functional groups such as carboxyl and phenolic groups. These similar functional groups might explain the resemblance adsorption curve of U(VI) on PANI/H-TNB in the presence of HA/FA.

3.7. Adsorption isotherms

The adsorption isotherms of U(VI) on PANI/H-TNB, H-TNB and PANI were displayed in Fig. 11. Higher adsorption capacities were observed for PANI/H-TNB composites than that of PANI and H-TNB due to the more active binding sites on PANI/H-TNB surface. It could also be seen that the uptake of U(VI) on PANI/H-TNB composites increased with the increasing solution concentrations. In order to quantify the adsorption data and understand the adsorption mechanism better, the experimental data were simulated by the Langmuir [44]and Freundlich models [45].

The Langmuir model was a theoretical model for the monolayer adsorption process. Its form can be described as follows

$$q_e = \frac{Lq_{\max}C_e}{1+LC_e} \tag{5}$$

And it can be converted into a linear form

$$\frac{C_e}{q_e} = \frac{C_e}{q_{\max}} + \frac{1}{Lq_{\max}} \tag{6}$$

Where q_{max} (mg/g) is the maximum capacity of U(VI) adsorbed on PANI/H-TNB and L (L/mg) is the Langmuir adsorption isotherm models constant.

The Freundlich isotherm model allowed for several types of adsorption on the solid and fitted the adsorption onto heterogeneity surface. This model can be defined as follows

$$q_e = k_f C_e^{\frac{1}{n}} \quad (7)$$

And it can also be converted into a linear form as

$$\log q_e = \frac{1}{n}\log C_e + \log K_f \quad (8)$$

k_f (mg^{1-n} L^n g^{-1}) is the Freundlich adsorption coefficient related to the adsorption capacity, and n represents the degree of dependence of adsorption with equilibrium concentration.

The fitted linear lines with the Langmuir and Freundlich models were plotted in Fig. 12a and 12b, respectively. The relative parameters calculated from the Langmuir and Freundlich models were displayed in Table 2. A comparison of the correlation coefficients (R^2) between the Langmuir and Freundlich models clearly indicated a better Langmuir model than Freundlich model, indicating a monolayer adsorption process. The q_{max} value calculated from the Langmuir model was 216.82 mg/g at 293 K, which is higher than other adsorbents, as listed in Table 3, indicating a potential promising adsorbent of PANI/H-TNB in the radioactive wastewater treatment.

3.8. Thermodynamic parameters

The adsorption amount of PANI/H-TNB composites increased with the increasing temperatures, as shown in Fig. 11, indicating an endothermic adsorption

process. The thermodynamic parameters (ΔG^0, ΔS^0 and ΔH^0) can be determined from the temperature-dependent adsorption isotherms. The values of thermodynamic parameters are obtained from the following equations:

$$\Delta G^0 = \Delta H^0 - T\Delta S^0 \quad (9)$$

$$\ln(\frac{q_e}{C_e}) = \frac{\Delta S^0}{R} - \frac{\Delta H^0}{RT} \quad (10)$$

$$k_0 = \frac{q_e}{C_e} \quad (11)$$

Where C_e (mg/L) is the equilibrium concentration, R (8.314 J mol^{-1} K^{-1}) is the universal constant and q_e(mg/g) is equilibrium adsorption capacity of U(VI).

The values of average standard enthalpy change (ΔH^0) and standard entropy change (ΔS^0) were derived from the slope and y-intercept of the plots of $\ln K_0$ versus 1/T (Fig. 13). The relative parameters calculated from the thermodynamic equations were illustrated in Table 4. The positive values of ΔH^0 confirmed an endothermic adsorption process, which can be explained by the competitive dissolution of U(VI) in water. The hydration sheaths of the U(VI) was supposed to be destroyed before its adsorption on PANI/H-TNB surfaces, and the energy required for this dehydration process exceeded the exothermicity of the ions attached to the surface, resulting in an endothermic adsorption process. Thus a higher temperature was favored. The negative ΔG^0 value suggested a spontaneous adsorption process. The value of ΔG^0 becoming more negative with the increasing temperature indicated that the adsorption process was more favorable at a higher temperature. The positive value of ΔS^0 indicated the high chemical affinity of PANI/H-TNB towards U(VI) ions as well as some structure

changes on the adsorbents [50]

3.9 Regeneration and reversibility

Taking into consideration of minimizing wastewater treatment cost and adsorbent secondary pollution, the reusability of PANI/H-TNB composites was also studied as a crucial factor for its potential application in the removal and recovery of U(VI). Uranium (VI)-loaded adsorbent was rinsed with 0.5 mol/L HCl, followed by deionized water, and dried at 60 °C for reuse. Fig. 14 illustrated adsorption capacities after each recycle. Specifically, the adsorption capacity decreased from 65.15 mg/g to 56.41 mg/g after 6 cycles. The excellent regeneration capacity indicated that the PANI/H-TNB composites had a potential application prospect as an effective absorbent for removal of U(VI) from large volumes of aqueous solutions.

4. Conclusions

In this work, batch experiments were employed to study the adsorption of U(VI) on PANI/H-TNB composites from aqueous solutions as a function of various experiment conditions such as contact time, solid content, pH value, foreign ions, and temperature. This adsorption process was strongly dependent on pH values, but ionic strength independent, suggesting an inner-sphere surface complexion mechanism. The adsorption process was observed to follow pseudo-second order kinetics and the adsorption isotherms could be fitted well by the Langmuir model. Thermodynamic data revealed a spontaneous and endothermic adsorption process. Moreover, the sorption capacity remained at a high level even after 6 cycles. The results in this study indicated that PANI/H-TNB composites could be used as a suitable absorbent for the

removal of uranium (VI) from contaminated wastewater.

Acknowledgment

The authors acknowledge the financial support from special scientific research fund of public welfare profession of China (201509074) and the National Natural Science Foundation of China (21575079).

References

1. B. Rasser, L. Desgranges and B. Pasquet, *Appl. Surf. Sci.*, 2003, **203**, 673-678.
2. D. S. Alessi, B. Uster, H. Veeramani, E. I. Suvorova, J. S. Lezama-Pacheco, J. E. Stubbs, J. R. Bargar and R. Bernier-Latmani, *Environ. Sci. Technol.*, 2012, **46**, 6150-6157.
3. M. Y. Zeng, Y. S Huang, S.W. Zhang, S. X. Qin, J. X. Li and J. Z. Xu, *RSC. Adv.*, 2014, **4**, 5021-5029.
4. H. Doi and T. Ito, *J. Nucl. Mater.*, 1964, **11**, 94-106.
5. L. M. Camacho, S. Deng and R. R. Parra, *J. Hazard. Mater*., 2010, **175**, 393-398.
6. D. D. Shao, X. X. Wang, J. X. Li, Y. S. Huang, X. M. Ren, G. S. Hou and X. K. Wang, *Environ. Sci.: Water Res. Technol.*, 2015, **1**, 169-176.
7. Z. J. Li, F. Chen, L. Y. Yuan, Y. L. Liu, Y. L. Zhao, Z. F. Chai and W. Q. Shi, *Chem. Eng. J., 2012*, **210**, 539-546.
8. Y. G. Zhao, J. X. Li, L. P. Zhao, S. W. Zhang, Y. S. Huang, X. L. Wu and X. K. Wang, *Chem. Eng. J.*, 2014, **235**, 275-283.

9. C. Kütahyalı and M. Eral, *Sep. Purif. Technol.*, 2004, **40**, 109-114.

10. Y. S. Huang and X. P. Chen, *Nano Life*, 2014, **4**, 1441006.

11. A. R. Hajipour, S. Habibi and A. E. Ruoho, *J. Appl. Polym. Sci.*, 2010, **118**, 818-826.

12. N. Wang, L. Zhou, J. Guo, Q. Ye, J.-M. Lin and J. Yuan, *Appl. Surf. Sci.*, 2014, **305**, 267-273.

13. L. G. He, Y. Liu, J. Z. Liu, Y. S. Xiong, J. Z. Zheng, Y. L. Liu and Z. Y. Tang, *Angew. Chem. Int. Edit.*, 2013, **52**, 3741-3745.

14. Y. Gao, C. L. Chen, H. Chen, R. Zhang and X. K. Wang, *Dalton .Trans.*, 2015, **44**, 8917-8925.

15. J. Pérez, L. Toledo, C. H. Campos, B. L. Rivas, J. Yañez and B. F. Urbano, *Chem. Eng. J.*, 2016, **287**, 744-754.

16. L. Wang, X.-L. Wu, W.-H. Xu, X.-J. Huang, J.-H. Liu and A.-W. Xu, *ACS. Appl. Mater. Interfaces.*, 2012, **4**, 2686-2692.

17. J. Li, Z. Y. Shao, C. L. Chen and X. K. Wang, *RSC. Adv.*, 2014, **4**, 38192-38198.

18. S. W. Zhang, M. Y. Zeng, W. Q. Xu, J. X. Li, J. Li, J. Z. Xu and X. K. Wang, *Dalton .Trans.*, 2013, **42**, 7854-7858.

19. S. Yunus, A. Attout and P. Bertrand, *Langmuir*, 2009, **25**, 1851-1854.

20. Y. Huang, J. Li, X. Chen and X. Wang, *RSC. Adv.*, 2014, **4**, 62160-62178.

21. D. D. Shao, G. S. Hou, J. X. Li, T. Wen, X. M. Ren and X. K. Wang, *Chem. Eng. J.*, 2014, **255**, 604-612.

22. D. J. Yang, Z. F. Zheng, H. W. Liu, H. Y. Zhu, X. B. Ke, Y. Xu, D. Wu and Y. Sun, *J. Phy. Chem. C*, 2008, **112**, 16275-16280.

23. C. Sanchez, B. Julian, P. Belleville and M. Popall, *J. Mater. Chem.*, 2005, **15**, 3559-3592.

24. H. Y. Zhu, X. P. Gao, Y. Lan, D. Y. Song, Y. X. Xi and J. C. Zhao, *J. Am. Chem. Soc.*, 2004, **126**, 8380-8381.

25. T. Wen, Q. H. Fan, X. L. Tan, Y. T. Chen, C. L. Chen, A. W. Xu and X. K. Wang, *Polym. Chem.*, 2016, **7**, 785-794.

26. J. S. Hu, L. S. Zhong, W. G. Song and L. J. Wan, *Adv. Mater.*, 2008, **20**, 2977-2982.

27. H. Y. Zhu, Y. Lan, X. P. Gao, S. P. Ringer, Z. F. Zheng, D. Y. Song and J. C. Zhao, *J. Am. Chem. Soc.*, 2005, **127**, 6730-6736.

28. Y. Z. Li, X. Zhao, Q. Xu, Q. H. Zhang and D. J. Chen, *Langmuir*, 2011, **27**, 6458-6463.

29. Y. B. Sun, D. D Shao, C. L. Chen, S. B. Yang and X. K. Wang, *Environ. Sci. Technol.*, 2013, **47**, 9904-9910.

30. J. Wang, B. L. Deng, H. Chen, X. R. Wang and J. Z. Zheng, *Environ. Sci. Technol.*, 2009, **43**, 5223-5228.

31. A. J. Francis, C. J. Dodge, F. Lu, G. P. Halada and C. R. Clayton, *Environ. Sci. Technol.* 1994, **28**, 636-639.

32. A. Kowal-Fouchard, R. Drot, E. Simoni and J. J. Ehrhardt, *Environ. Sci. Technol.*, 2004, **38**, 1399-1407.

33. Y. G. Zhao, J. X. Li, S. W. Zhang and X. K. Wang, *RSC. Adv.*, 2014, **4**, 32710-32717.

34. Y.-S. Ho and A. E. Ofomaja, *J. Hazard. Mater.*, 2006, **137**, 1796-1802.

35. Y.-S. Ho, *J. Hazard. Mater.*, 2006, **136**, 681-689.

36. W. C. Song, M. C. Liu, R. Hu, X. L. Tan and J. X. Li, *Chem. Eng. J.*, 2014, **246**, 268-276.

37. Z. W. Zhao, J. X. Li, T. Wen, C. C. Shen, X. K. Wang and A. Xu, *Colloid. Surface. A*, 2015,**482**, 258-266.

38. X. Liu, J. X. Li, X. X. Wang, C. L. Chen and X. K. Wang, *J. Nucl. Mater.*, 2015, **466**, 56-64.

39. S. P. Hyun, J. A. Davis, K. Sun and K. F. Hayes, *Environ. Sci. Technol.*, 2012, **46**, 3369-3376.

40. J. X. Li, J. Hu, G. D. Sheng, G. X. Zhao and Q. Huang, *Colloid. Surface. A*, 2009, **349**, 195-201.

41. G. D. Sheng, S. W. Wang, J. Hu, Y. Lu, J. X. Li, Y. H. Dong and X. K. Wang, *Colloid. Surface. A*, 2009, **339**, 159-166.

42. X. M. Ren, S. W. Wang, S. T. Yang and J. X. Li, *J. Radioanal. Nucl. Chem.*, 2010, **283**, 253-259.

43. S. W. Wang, J. Hu, J. X. Li and Y. H. Dong, *J. Hazard. Mater.*, 2009, **167**, 44-51.

44. I. Langmuir, J. Am. Chem. Soc., 1918, **40**, 1361-1403.

45. H.M.F. Frendlich, *J. Phys. Chem*, 1906, **57**, 385-407.

46. Y. H. Liu, Q. Li, X. H. Cao, Y. Q. Wang, X. H. Jiang, M. Li, M. Hua and Z. B. Zhang, *Appl. Surf. Sci.*, 2013, **285**, 258-266.

47. S. Şimşek and U. Ulusoy, *J. Radioanal. Nucl. Chem.*, 2012, **292**, 41-51.

48. J. X. Li, Z. Q. Guo, S. W. Zhang and X. K. Wang, *Chem. Eng. J.*, 2011, **172**, 892-897.

49. L. C. Tan, X. F. Zhang, Q. Liu, X. Y. Jing, J. Y. Liu, D. L. Song, S. X. Hu, L. H. Liu and J. Wang, *Colloid. Surface. A*, 2015, **469**, 279-286.

50. G. X. Zhao, J. X. Li, X. M. Ren, C. L. Chen and X. K. Wang, *Environ. Sci. Technol.*, 2011, **45**, 10454-10462.

Figure Captions

Fig.1. SEM images of bare PANI nanorods (a) and PANI/H-TNB (b); TEM images of bare PANI nanorods (c) and PANI/H-TNB (d).

Fig. 2. XRD patterns of H-TNB, PANI and PANI/H-TNB.

Fig. 3. FTIR spectra of H-TNB, PANI and PANI/H-TNB.

Fig. 4. The XPS survey for the PANI/H-TNB after adsorption (a), U 4f (b)

Fig. 5. The zeta potential of PANI and PANI/H-TNB, T = 293 K, m/V = 0.3 g/L.

Fig. 6. Adsorption kinetics of U(VI) on PANI/H-TNB surface. T = 293 K, m/V = 0.3 g/L, C_0 = 20 mg/L, I = 0.01 mol/L $NaNO_3$, pH = 5.0 ± 0.1.

Fig. 7. Effect of adsorbent content on U(VI) adsorption on PANI/H-TNB surface, C_0 = 20 mg/L1, I = 0.01 mol/L $NaNO_3$, pH = 5.0 ± 0.1.

Fig. 8. Effect of pH and ionic strength on U(VI) adsorption on PANI/H-TNB T = 293 K, m/V = 0.3 g/L, C_0 = 20 mg/L.

Fig. 9. Effect of coexisting electrolyte cations (a) and anions (b) on U(VI) adsorption to PANI/H-TNB, T = 293 K, m/V = 0.3 g/L, C_0 = 20 mg/L.

Fig. 10. Effect of HA/FA on the adsorption of U(VI) on PANI/H-TNB as a function of pH, m/V = 0.3 g/L, C_0 = 20 mg/L, I = 0.01 mol/L $NaNO_3$, T = 293 K.

Fig. 11. Adsorption isotherms of U(VI) ions on PANI/H-TNB, H-TNB and PANI. m/V = 0.3 g/L, pH = 5.0 ± 0.1, I = 0.01 mol/L $NaNO_3$. Symbols denote experimental data, the solid lines represent Langmuir model simulation, the dotted lines represent the Freundlich model.

Fig. 12. Langmuir (a) and Freundlich (b) simulation for the adsorption isotherms of U(VI) on PANI/H-TNB at three different temperatures, m/V = 0.3 g/L, pH = 5.0 ± 0.1,

I = 0.01 mol/L $NaNO_3$.

Fig. 13. Plots of lnk_0 versus 1/T for U(VI) adsorption on PANI/H-TNB. m/V = 0.3 g/L, pH = 5.0 ± 0.1, I = 0.01 mol/L $NaNO_3$.

Fig. 14. Recycling of PANI/H-TNB for the removal of U(VI). C_0 = 20 mg/L, pH = 5.0 ± 0.1, m/V = 0.3 g/L, I = 0.01 mol/L $NaNO_3$ and T = 293 K.

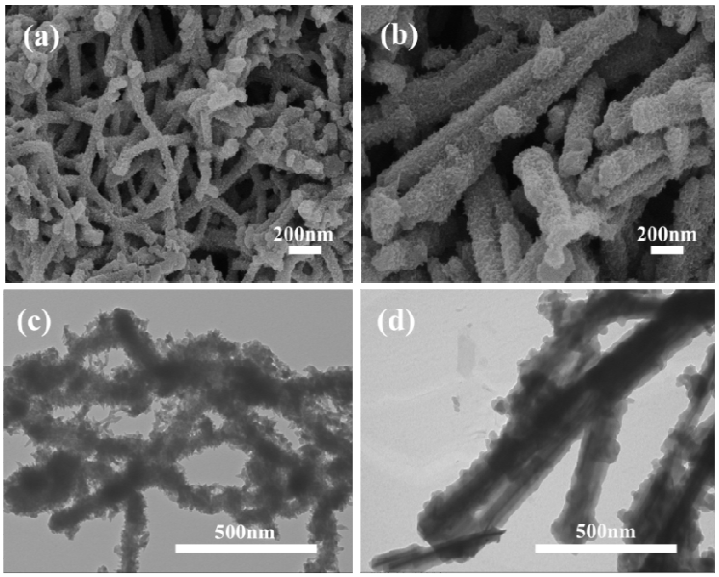

Fig.1.

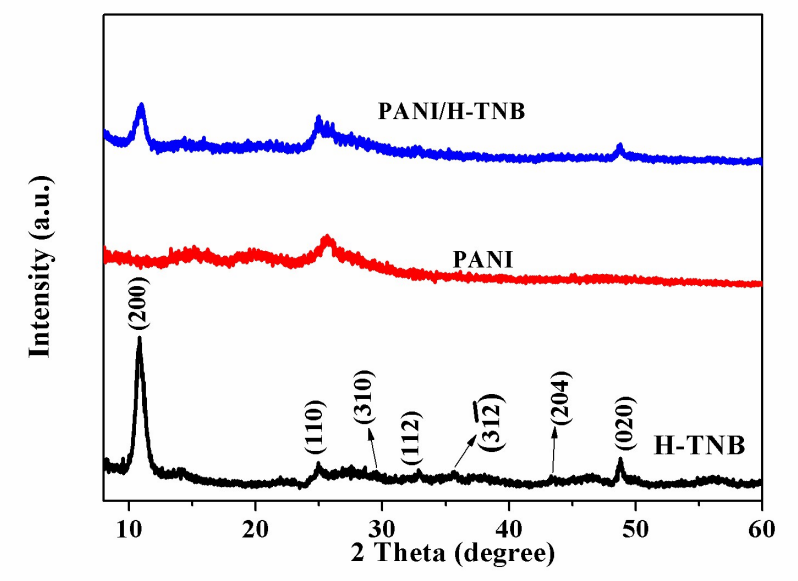

Fig.2.

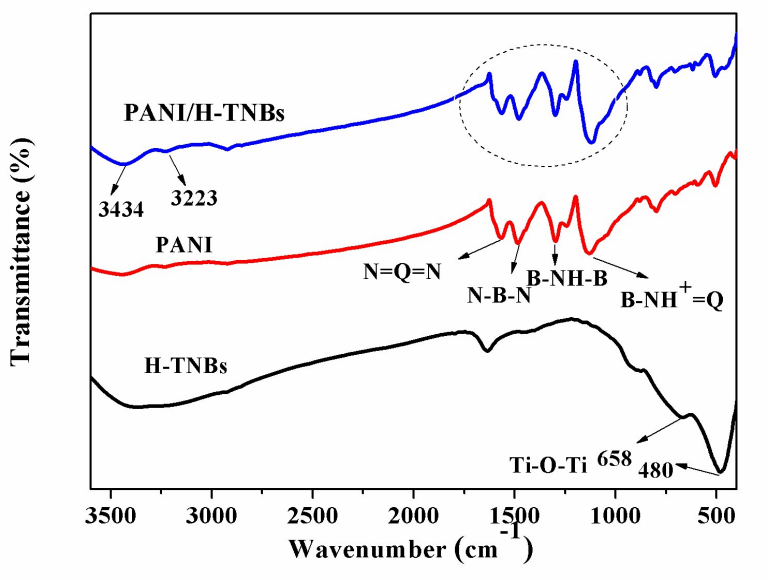

Fig.3.

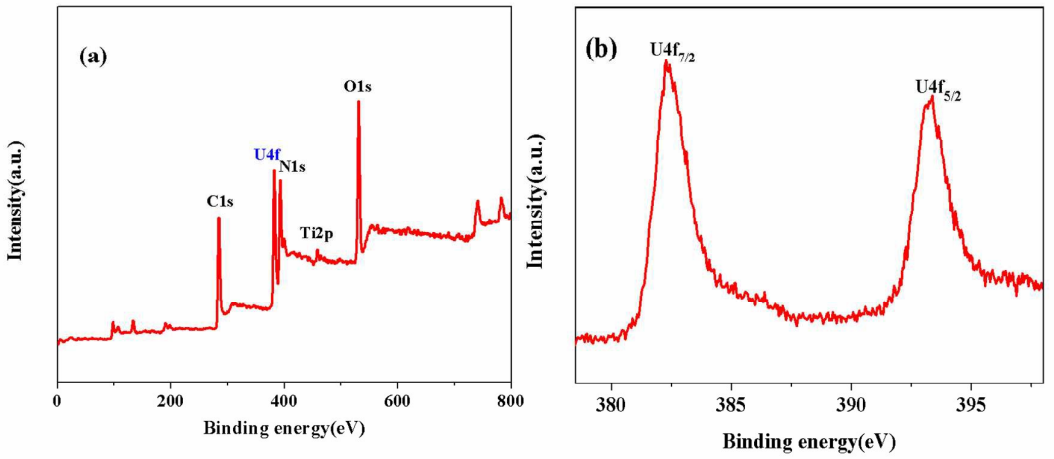

Fig.4.

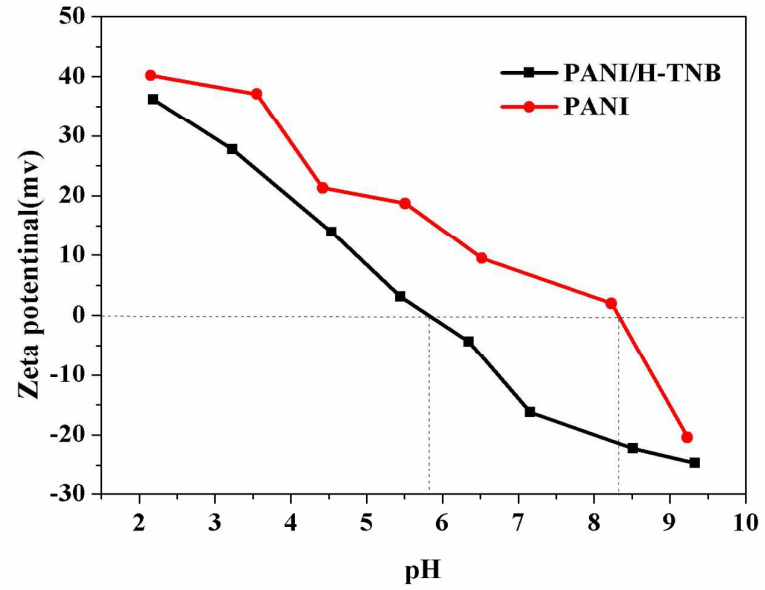

Fig.5.

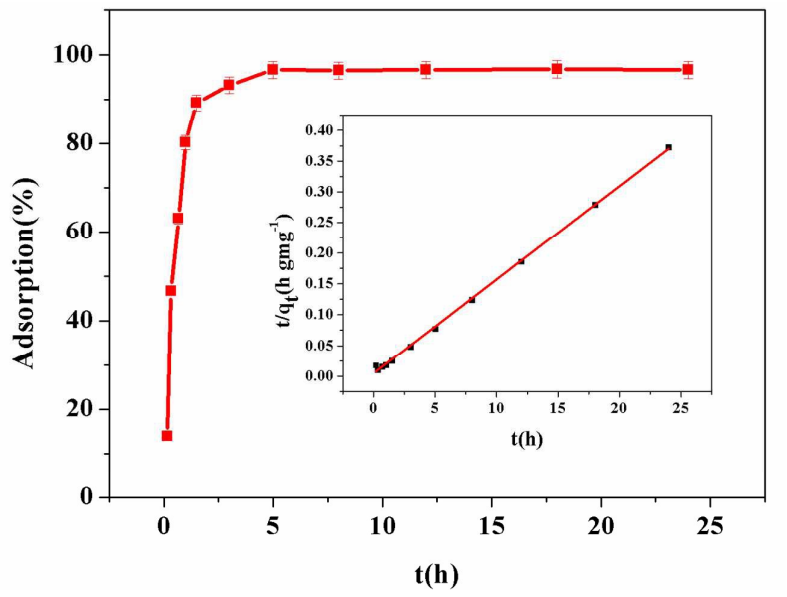

Fig.6.

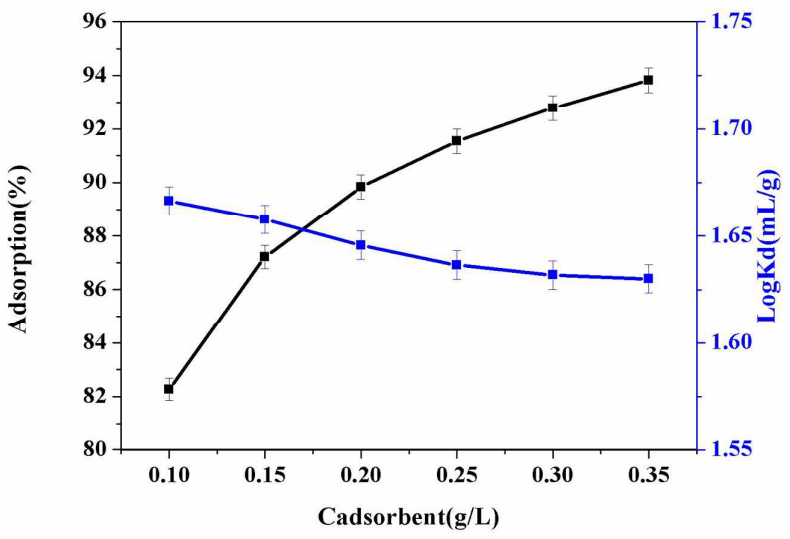

Fig.7.

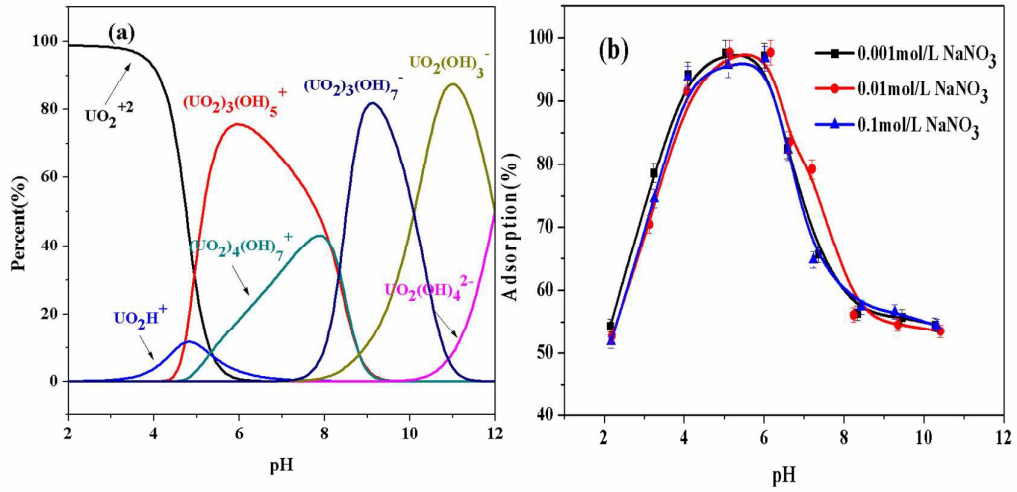

Fig.8.

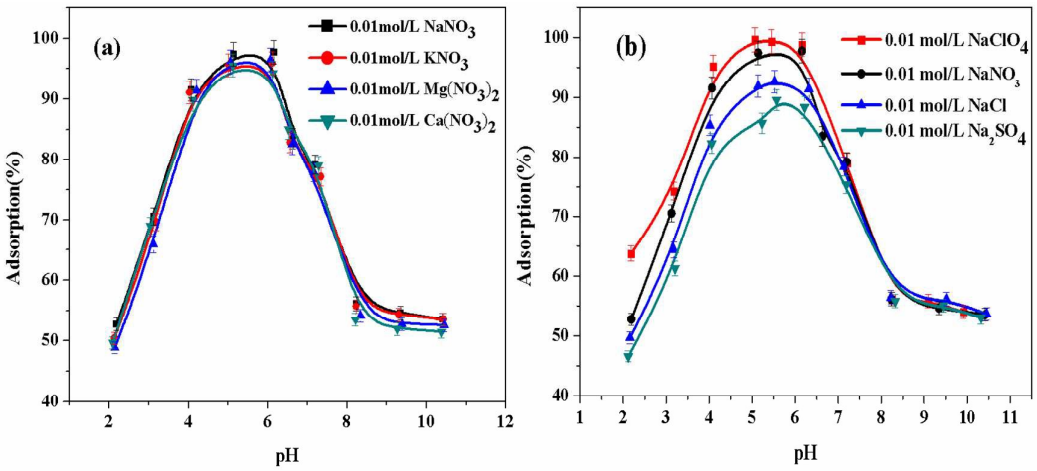

Fig.9.

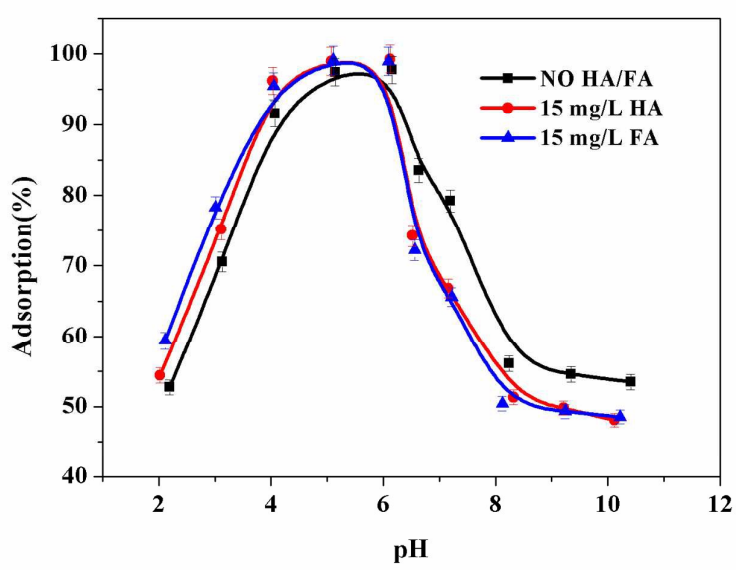

Fig.10.

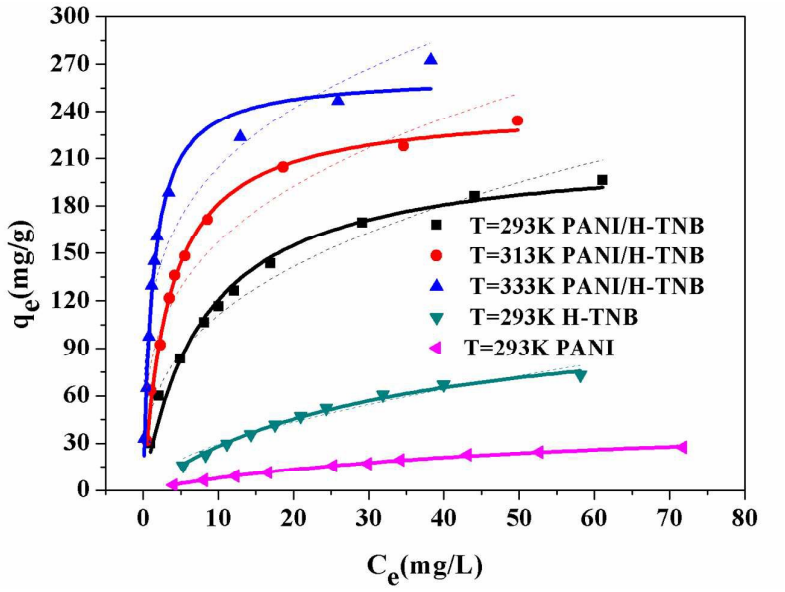

Fig.11.

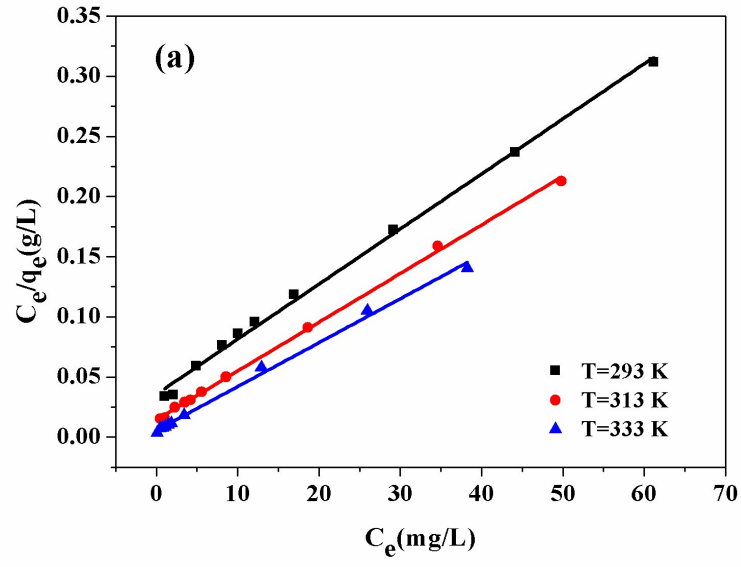

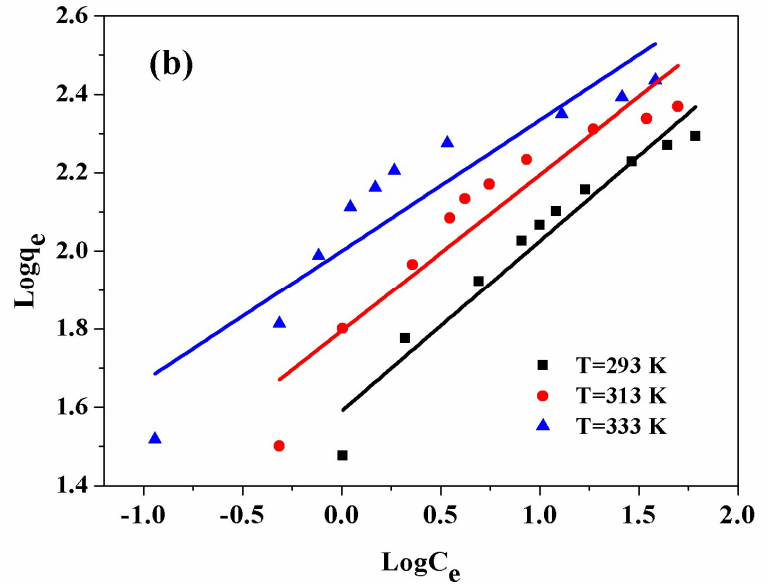

Fig.12.

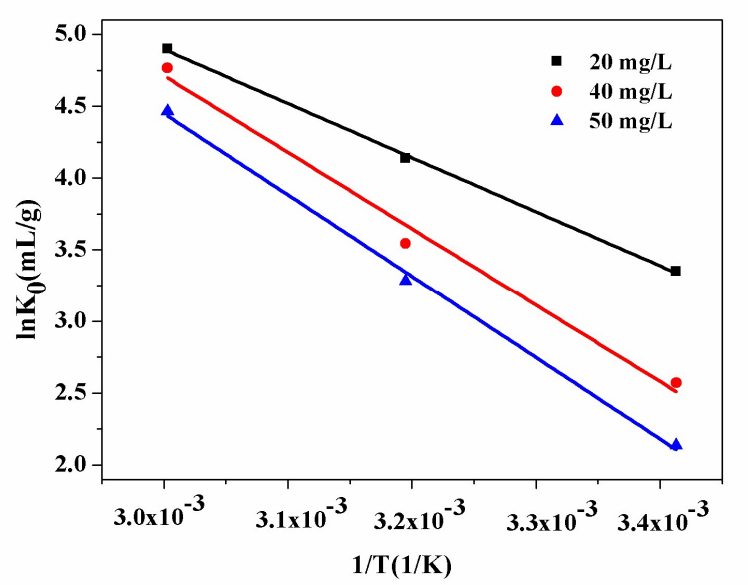

Fig.13.

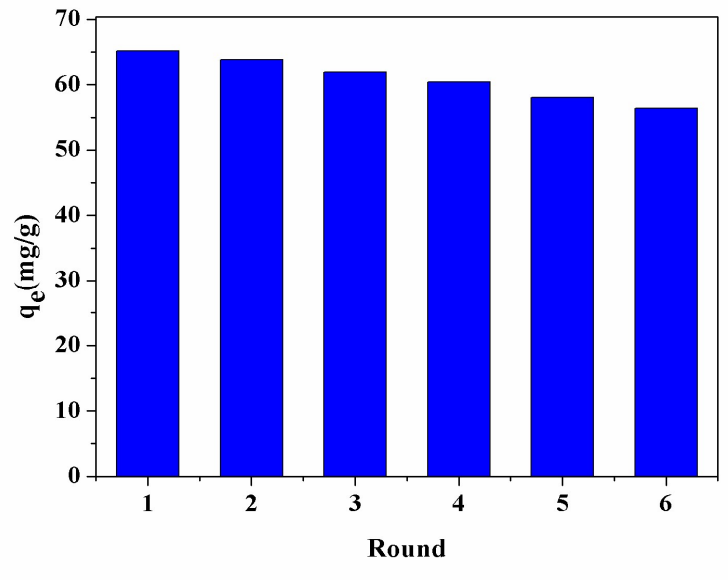

Fig.14.

Table 1 Kinetic model parameters for the adsorption of on PANI/H-TNB composites.

	Pesudo-first-order kinetic model			Pesudo-second-order kinetic model		
C_0(mg/L)	q_e(mg/g)	k_1(h^{-1})	R^2	q_e(mg/g)	k_2(g/(mg h))	R^2
20	101.42	1.44	0.885	65.79	0.05	0.999

Table 2 The parameters of Langmuir and Freundlich models simulation the adsorption isotherms of U(VI) on PANI/H-TNB composites.

sorbents	Langmuir				Freundlich		
	T (K)	L (L/mg)	q_{max} (mg/g)	R^2	n	K_f ($mg^{1-n} L^n g^{-1}$)	R^2
PANI	293	0.02	48.75	0.997	0.63	1.95	0.980
H-TNB	293	0.03	116.73	0.992	0.56	8.03	0.956
PANI/H-TNB	293	0.13	216.82	0.985	0.35	49.61	0.964
	313	0.29	243.77	0.996	0.29	80.25	0.915
	333	0.80	263.02	0.982	0.24	116.79	0.903

Table 3 Comparison of maximum adsorption capacity of U(VI)with other adsorbents.

Adsorbent	Experiment condition	Adsorption capacity(mg/g)	Reference
PANI–CMK-3	T = 298 K, pH = 7.0	118.30.	46
PANI@GO	T = 298 K, pH = 3.0	245.14	29
Amidoxime modified Fe_3O_4@SiO_2	T = 298 K, pH = 5.0	105.00	8
Amidoxime modified bentonite	T =298 K, pH = 4.0	33.30	47
Fe_3O_4@Agarose microsphere	T = 293 K, pH = 5.2	273.94	48
Fe_3O_4@TiO_2	T = 298 K, pH = 6.0	91.10	49
PANI/H-TNB	T = 293 K, pH = 5.0	216.82	In this work

Table 4 Thermodynamic parameters for U(VI) adsorption on PANI/H-TNB composites.

C_0 (mg/L)	ΔH^0 (kJ mol^{-1})	ΔS^0 ($Jmol^{-1}$ K^{-1})	ΔG^0(kJ mol^{-1}) 293 K	313 K	333K
20	30.77	134.75	-8.71	-11.41	-14.10
40	44.34	172.21	-6.09	-9.56	-13.01
50	47.19	178.56	-5.13	-8.70	-12.27

Graphical Abstract